PERGAMON

International Journal of Solids and Structures 40 (2003) 2401–2419

INTERNATIONAL JOURNAL OF SOLIDS and STRUCTURES

www.elsevier.com/locate/ijsolstr

Special virtual fields for the direct determination of material parameters with the virtual fields method. 3. Application to the bending rigidities of anisotropic plates

Michel Grédiac [a,*], Evelyne Toussaint [a], Fabrice Pierron [b]

[a] *Laboratoire d'Etudes et de Recherches en Mécanique des Structures, Université Blaise Pascal Clermont II, 24, avenue des Landais, BP 206, 63174 Aubière Cedex, France*

[b] *Laboratoire de Mécanique et Procédés de Fabrication, Ecole Nationale Supérieure des Arts et Métiers, rue Saint-Dominique, BP 508, 51006 Châlons-en-Champagne Cedex, France*

Received 26 June 2002; received in revised form 4 December 2002

Abstract

This paper deals with the direct identification of bending rigidities of thin anisotropic plates. These parameters are extracted from an heterogeneous strain field which takes place onto the top surface of a bent plate. The loading conditions are such that no closed-form solution is available for the deflection/slope/curvature fields. The procedure presently used is the virtual fields method with "special" virtual fields. It is shown that the unknown parameters are directly extracted with this method since no iterative calculations are required. The parameters are in fact directly equal to the virtual work of the applied loading with the special virtual displacement fields. The headlines of the method are recalled in the first part of the paper. They are then applied in the case of anisotropic bent plates. The accuracy and the stability of the procedure are finally discussed through some relevant examples.

Keywords: Anisotropy; Bending; Composites; Identification; Inverse problem; Virtual fields method

1. Introduction

This work deals with the identification of the six bending rigidities of thin anisotropic plates from the heterogeneous strain field which takes place onto the top surface of a bent plate. The interest lies in the fact that the whole set of unknown parameters is involved in the mechanical response of the tested specimen. Consequently, one test only is carried out for determining several parameters. The drawback of such approaches is generally the fact that no closed-form solutions for the strain/stress fields are available. Suitable methods based on the updating of numerical models are generally proposed to solve this problem, especially when natural frequencies are considered as input data (Sol, 1986; Deobald and Gibson, 1988;

* Corresponding author. Tel.: +33-4-73-40-75-29; fax: +33-4-73-40-74-94.
E-mail address: grediac@lermes.univ-bpclermont.fr (M. Grédiac).

0020-7683/02/$ - see front matter © 2002 Elsevier Science Ltd. All rights reserved.
doi:10.1016/S0020-7683(03)00030-1

DeWilde, 1990; Ayorinde and Gibson, 1993; Mota Soares et al., 1993; Araujo et al., 1996; Frederiksen, 1997; Okada et al., 1999). Such an approach has also been used in the case of static tests, either for in-plane (Hendricks, 1991; Meuwissen et al., 1998; Okada et al., 1999) or bending tests (Wang and Kam, 2001; LeMagorou et al., 2002). Another method which departs from the above ones is to avoid the iterative updating of numerical models with a *direct* identification of the unknown parameters (Grédiac, 1989). In this last approach, it is shown that the measured fields can be processed with a suitable use of the well-known principle of virtual work (PVW) which describes the global equilibrium of the tested specimen. This method is called the virtual fields method (VFM). Indeed, writing the PVW with particular virtual fields leads in some cases (among which the anisotropic linear elasticity) to a system of linear equations from which the unknown parameters are extracted after inversion. This approach has been successfully used in the last decade in different cases of anisotropic material characterization (see for instance Grédiac and Vautrin, 1990; Grédiac, 1996a; Grédiac, 1996b; Grédiac and Pierron, 1998; Grédiac et al., 1999; Pierron et al., 2000; Pierron and Grédiac, 2000; Grédiac et al., 2001). With this approach, the key-point is the choice of the virtual fields. In the above studies, this choice was somewhat empirical. In a companion paper, a dramatic improvement has been proposed with the automatic construction of so-called *special* virtual fields (Grédiac et al., 2002a). In this work, the choice of the virtual fields is no more empirical but obtained with an automatic procedure. This "revisited" VFM has been successfully used for the determination of in-plane properties of an orthotropic material, either in linear elasticity or in some cases of non-linearities (Grédiac et al., 2002b). The objective here is to study the capabilities of the VFM with special virtual fields in the case of the determination of bending rigidities of thin anisotropic plates. The theoretical aspects of the method are described in the first part of the paper. A procedure for automatically constructing the special virtual fields is then presented. Finally, some numerical examples of identifications illustrate the accuracy and the stability of the VFM with special virtual fields for finding the bending rigidities of thin anisotropic plates.

2. Theory

Let us consider a bent plate of any shape (see Fig. 1). It is subjected to n_f forces F_i, $i = 1, \ldots, n_f$ at points $M_i(x_i, y_i)$, $i = 1, \ldots, n_f$. It is simply supported at n_s different points $P_i(x'_i, y'_i)$, $i = 1, \ldots, n_s$. V, S and e are respectively the volume, the external surface and the thickness of the plate. Within the framework of the theory of anisotropic plates (Lekhnitskii, 1968), the moment/curvature relations may be written as (with the usual rule of contracted indices: $xx \to x$, $yy \to y$, $xy \to s$)

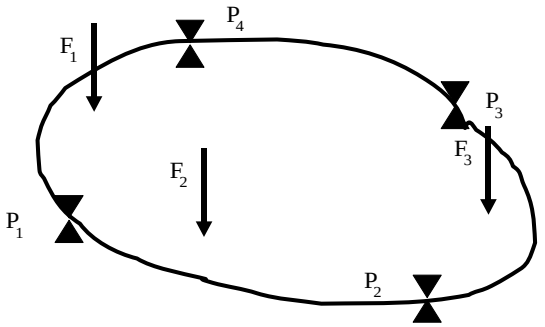

Fig. 1. Plate of any shape.

$$\begin{bmatrix} M_x \\ M_y \\ M_s \end{bmatrix} = \begin{bmatrix} D_{xx} & D_{xy} & D_{xs} \\ D_{xy} & D_{yy} & D_{ys} \\ D_{xs} & D_{ys} & D_{ss} \end{bmatrix} \begin{bmatrix} k_x \\ k_y \\ k_s \end{bmatrix} \tag{1}$$

where the M_i's are the bending moments, the D_{ij}'s are the bending stiffnesses, the k_i's are the curvatures defined by

$$\begin{cases} k_x = -\dfrac{\partial^2 w}{\partial x^2} \\ k_y = -\dfrac{\partial^2 w}{\partial y^2} \\ k_s = -2\dfrac{\partial^2 w}{\partial x \partial y} \end{cases} \tag{2}$$

where w is the deflection.

The goal here is to identify the D_{ij}'s from the heterogeneous curvature fields which takes place on the top surface of the bent plate assuming that no closed-form solution for these fields is available. Within the framework of the theory of thin plates, the global equilibrium of the plate can be written with the PVW

$$I_{xx}D_{xx} + I_{yy}D_{yy} + I_{xy}D_{xy} + I_{ss}D_{ss} + I_{xs}D_{xs} + I_{ys}D_{ys} = W_e^* \tag{3}$$

The I_{ij}'s are defined by

$$\begin{cases} I_{xx} = \int_S k_x k_x^* \, \mathrm{d}S \\ I_{yy} = \int_S k_y k_y^* \, \mathrm{d}S \\ I_{xy} = \int_S (k_x k_y^* + k_y k_x^*) \, \mathrm{d}S \\ I_{ss} = \int_S k_s k_s^* \, \mathrm{d}S \\ I_{xs} = \int_S (k_x k_s^* + k_s k_x^*) \, \mathrm{d}S \\ I_{ys} = \int_S (k_y k_s^* + k_s k_y^*) \, \mathrm{d}S \end{cases} \tag{4}$$

and W_e^* is the virtual work produced by the n_f applied loading forces F_j, $j = 1, \ldots, n_f$

$$W_e^* = \sum_{j=1}^{j=n_f} F_j u^*(x_j, y_j) \tag{5}$$

The VFM consists in writing the above equation of global equilibrium with some particular virtual fields $\mathbf{w}^*$ (Grédiac, 1989). If as many different virtual fields as unknown parameters are found, a linear system is obtained and inverted to get the unknowns.

The key-point of the method is the choice of the virtual fields since one has to choose among an infinite number of possibilities. In the previous studies dealing with the VFM (Grédiac and Vautrin, 1990; Grédiac, 1996a; Grédiac, 1996b; Grédiac and Pierron, 1998; Grédiac et al., 1999; Pierron et al., 2000; Pierron and Grédiac, 2000; Grédiac et al., 2001), those fields were chosen intuitively or following some semi-empirical rules. For instance, the virtual fields were such that some components in the matrix of the linear system were zero. Then the linear equations were partially uncoupled. In a companion paper (Grédiac et al., 2002a), it is shown that some virtual fields called *special* virtual fields render the matrix of the linear system equal to unity, leading therefore to a direct identification of the unknown parameters. These special virtual fields are denoted hereafter $\widehat{\mathbf{w}}^*$. The idea is to use the PVW with those special virtual fields such that five of the six I_{ij}'s are zero whereas the sixth one is equal to one. This leads to a direct determination of the parameter which coefficient is 1 in Eq. (6). For instance, if D_{xx} is the parameter to be extracted from the heterogeneous actual field, one can write

$$\underbrace{I_{xx}}_{=1} D_{xx} + \underbrace{I_{yy}}_{=0} D_{yy} + \underbrace{I_{xy}}_{=0} D_{xy} + \underbrace{I_{ss}}_{=0} D_{ss} + \underbrace{I_{xs}}_{=0} D_{xs} + \underbrace{I_{ys}}_{=0} D_{ys} = W_e^* \tag{6}$$

The other unknowns are found by moving the "1" from one I_{ij} to another. Since six material parameters are to be determined, the problem is eventually to find six special virtual fields $\widehat{\mathbf{w}}^{*(i)}$, $i = 1, \ldots, 6$ such that the equalities in Table 1 are verified. In each case, the unknown parameter is equal to the virtual work of the applied loading. Thus

$$\begin{cases} D_{xx} = W_e^{*(1)} \\ D_{yy} = W_e^{*(2)} \\ D_{xy} = W_e^{*(3)} \\ D_{ss} = W_e^{*(4)} \\ D_{xs} = W_e^{*(5)} \\ D_{ys} = W_e^{*(6)} \end{cases} \tag{7}$$

with

$$W_e^{*(i)} = \sum_{j=1}^{j=n_f} F_j \widehat{w}^{*(i)}(x_j, y_j) \tag{8}$$

In Grédiac et al. (2002a), a general procedure for constructing the special virtual fields is proposed. The aim here is to examine the practical implementation of this procedure and its efficiency in the case of bent plates.

3. Construction of the special virtual fields

3.1. Constraints under which the special virtual fields must be built

Let us now examine the properties that the special virtual fields $\widehat{\mathbf{w}}^*$ must satisfy. As explained in Grédiac et al. (2002a), these fields must obey two conditions in all cases. Three extra conditions must also be satisfied if the distribution of the loading remains unknown or if only one part of the actual strain field is measured but these particular conditions do not hold here. The two first conditions are

- *Condition 1:* the special virtual fields must be kinematically admissible. Hence,

$$\forall j = 1, \ldots, n_s, \widehat{w}^*(x'_j, y'_j) = 0 \tag{9}$$

- *Condition 2:* for each unknown stiffness, the special virtual fields must verify the six fundamental equalities in Table 1.

Table 1
Value of the different integrals with the special virtual fields

Extracted parameter	Special virtual field	I_{xx}	I_{yy}	I_{xy}	I_{ss}	I_{xs}	I_{ys}
D_{xx}	$\widehat{\mathbf{w}}^{*(1)}$	1	0	0	0	0	0
D_{yy}	$\widehat{\mathbf{w}}^{*(2)}$	0	1	0	0	0	0
D_{xy}	$\widehat{\mathbf{w}}^{*(3)}$	0	0	1	0	0	0
D_{ss}	$\widehat{\mathbf{w}}^{*(4)}$	0	0	0	1	0	0
D_{xs}	$\widehat{\mathbf{w}}^{*(5)}$	0	0	0	0	1	0
D_{ys}	$\widehat{\mathbf{w}}^{*(6)}$	0	0	0	0	0	1

3.2. General expression of the virtual fields

According to Grédiac et al. (2002a), it is proposed to expand the special virtual deflection with monomials as follows

$$\widehat{w}^* = \sum_{i=0}^{m} \sum_{j=0}^{n} A_{ij} \left(\frac{x}{a}\right)^i \left(\frac{y}{b}\right)^j \tag{10}$$

where the A_{ij}'s are unknown coefficients which completely define the special virtual deflection fields and therefore the corresponding unknown stiffness. The number of these unknowns is denoted n_{unk}, with

$$n_{\text{unk}} = (n+1) \times (m+1) \tag{11}$$

The goal is now to determine the n_{unk} A_{ij}'s using the above two conditions.

3.2.1. Condition 1

The plate is simply supported at n_s points $P_k(x'_k, y'_k)$. Hence condition 1 and Eq. (10) lead to n_s linear equations of the type

$$\sum_{i=0}^{m} \sum_{j=0}^{n} A_{ij} \left(\frac{x'_k}{a}\right)^i \left(\frac{y'_k}{b}\right)^j = 0, \quad k = 1, \ldots, n_s \tag{12}$$

Note that one could also consider the following virtual deflection field instead of the preceding one defined in Eq. (10)

$$\widehat{w}^* = \prod_{k=0}^{n_s} (x - x'_k)(y - y'_k) \left(\sum_{i=0}^{m} \sum_{j=0}^{n} A_{ij} \left(\frac{x}{a}\right)^i \left(\frac{y}{b}\right)^j \right) \tag{13}$$

Such a field is directly kinematically admissible, but the calculation of the virtual strain components is much more complicated in this last case. Consequently, the field in Eq. (10) is used in the following.

3.2.2. Condition 2

Integrals which appear in the six fundamental equalities in Table 1 involve the special virtual curvatures. These curvatures are deduced from the special virtual deflection field $\widehat{w}^*$ by differentiation

$$\begin{cases} \widehat{k}_x^* = -\frac{1}{a^2} \left(\sum_{i=2}^{m} \sum_{j=0}^{n} i(i-1) A_{ij} \left(\frac{x}{a}\right)^{(i-2)} \left(\frac{y}{b}\right)^j \right) \\ \widehat{k}_y^* = -\frac{1}{b^2} \left(\sum_{i=0}^{m} \sum_{j=2}^{n} j(j-1) A_{ij} \left(\frac{x}{a}\right)^i \left(\frac{y}{b}\right)^{(j-2)} \right) \\ \widehat{k}_s^* = -\frac{2}{ab} \left(\sum_{i=1}^{m} \sum_{j=1}^{n} ij A_{ij} \left(\frac{x}{a}\right)^{(i-1)} \left(\frac{y}{b}\right)^{(j-1)} \right) \end{cases} \tag{14}$$

Substituting the above expressions of the virtual curvature components in the six equalities provides six linear equations where the A_{ij}'s are the unknowns. These equations are not reported here for the sake of legibility.

3.3. Final linear system

In conclusion of the above section, a system of $n_s + 6$ linear equations where the A_{ij}'s are the unknowns is obtained. For instance, the n_{unk} A_{ij}'s of a special virtual field leading to D_{11} verify the following system

$$\left\{\begin{array}{l|l}
\frac{1}{a^2}\sum_{i=2}^{m}\sum_{j=0}^{n}A_{ij}i(i-1)\int_S k_x\left(\frac{x}{a}\right)^{(i-2)}\left(\frac{y}{b}\right)^{j}\mathrm{d}S = 1 & \\
\frac{1}{b^2}\sum_{i=0}^{m}\sum_{j=2}^{n}A_{ij}j(j-1)\int_S k_y\left(\frac{x}{a}\right)^{i}\left(\frac{y}{b}\right)^{(j-2)}\mathrm{d}S = 0 & \\
\frac{1}{b^2}\sum_{i=0}^{m}\sum_{j=2}^{n}A_{ij}j(j-1)\int_S k_x\left(\frac{x}{a}\right)^{i}\left(\frac{y}{b}\right)^{(j-2)}\mathrm{d}S & \\
\quad+\frac{1}{a^2}\sum_{i=2}^{m}\sum_{j=0}^{n}A_{ij}i(i-1)\int_S k_y\left(\frac{x}{a}\right)^{(i-2)}\left(\frac{y}{b}\right)^{j}\mathrm{d}S = 0 & \\
\frac{1}{ab}\sum_{i=1}^{m}\sum_{j=1}^{n}A_{ij}ij\int_S k_s\left(\frac{x}{a}\right)^{(i-1)}\left(\frac{y}{b}\right)^{(j-1)}\mathrm{d}S = 0 & 6\text{ equations} \\
\frac{1}{ab}\sum_{i=1}^{m}\sum_{j=1}^{n}A_{ij}ij\int_S k_x\left(\frac{x}{a}\right)^{(i-1)}\left(\frac{y}{b}\right)^{(j-1)}\mathrm{d}S & \\
\quad+\frac{1}{a^2}\sum_{i=2}^{m}\sum_{j=0}^{n}A_{ij}i(i-1)\int_S k_s\left(\frac{x}{a}\right)^{i-2}\left(\frac{y}{b}\right)^{j}\mathrm{d}S = 0 & \\
\frac{1}{ab}\sum_{i=1}^{m}\sum_{j=1}^{n}A_{ij}ij\int_S k_y\left(\frac{x}{a}\right)^{(i-1)}\left(\frac{y}{b}\right)^{(j-1)}\mathrm{d}S & \\
\quad+\frac{1}{b^2}\sum_{i=0}^{m}\sum_{j=2}^{n}A_{ij}j(j-1)\int_S k_s\left(\frac{x}{a}\right)^{i}\left(\frac{y}{b}\right)^{(j-2)}\mathrm{d}S = 0 & \\
\hline
\sum_{i=0}^{m}\sum_{j=0}^{n}A_{ij}\left(\frac{x_1}{a}\right)^{i}\left(\frac{y_1}{b}\right)^{j} = 0 & \\
\sum_{i=0}^{m}\sum_{j=0}^{n}A_{ij}\left(\frac{x_2}{a}\right)^{i}\left(\frac{y_2}{b}\right)^{j} = 0 & n_s\text{ equations} \\
\vdots & \\
\sum_{i=0}^{m}\sum_{j=0}^{n}A_{ij}\left(\frac{x_{n_s}}{a}\right)^{i}\left(\frac{y_{n_s}}{b}\right)^{j} = 0 &
\end{array}\right. \tag{15}$$

The A_{ij}'s of the special virtual fields leading to the other stiffness parameters are determined by changing the location of the "1" in the right-hand part of the system. The above system can be written as

$$\mathbf{DY} = \mathbf{E} \tag{16}$$

where $\mathbf{D}$ is a $(6 + n_s) \times n_{\text{unk}}$ rectangular matrix, $\mathbf{Y}$ is the vector of the n_{unk} unknown A_{ij}'s which define the special virtual fields, $\mathbf{E}$ is a vector with $6 + n_s$ components. All of them are equal to 0 except one among the six first ones which is equal to 1. As explained above, the location of this 1 depends on the stiffness to be determined. Let us now examine the procedure used for solving this system.

3.4. Procedure used for solving the final linear system

The procedure presently used for solving the system is described in Grédiac et al. (2002a) and Grédiac and Pierron (2001). Only its main characteristics are therefore recalled.

It must first be underlined that there are more unknowns than equations if the expansion of the virtual field in Eq. (10) is such that

$$n_{\text{unk}} > 6 + n_s \tag{17}$$

In this case, the matrix of the linear system becomes rectangular and there is an infinity of solutions. The idea is to take advantage of this property to retain a solution which is the most stable when noisy data are considered. First the

$$\frac{n_{\text{unk}}!}{(6+n_s)!(n_{\text{unk}}-6-n_s)!}$$

different $(6+n_s)\times(6+n_s)$ square matrices are extracted. It is then examined if the corresponding linear system can be inverted, i.e. if the determinant is different from zero. In this case, the $(6+n_s)$ corresponding A_{ij}'s are determined by inversion of the linear system assuming that the remaining $n_{\text{unk}}-6-n_s$ A_{ij}'s are zero for stability reasons (Grédiac et al., 2002a). A special virtual field is obtained and the corresponding unknown stiffness if deduced using Eq. (7). Since many different invertible square matrices are found in practice, several estimates of the stiffnesses are obtained. It is considered that the "best" estimate is the value which is the less sensitive to noisy data (Grédiac et al., 2002a). Selecting the square matrix with the best condition number could be considered (Golub and Loan, 1993), but it has been shown that it is more efficient to *voluntary* introduce a disturbance in the input data (Grédiac and Pierron, 2001) and then to select the estimate which is the less sensitive to this disturbance. The reason is the fact that the method of the condition number is too general: it does not account for the particular structure of the components of the matrix. Since they are built as weighted integrals of the actual measured strain fields, they do not uniformly react when a noise is introduced. Finally, all the invertible square matrices are disturbed (presently by adding a constant value to the coordinates) and new stiffnesses are deduced. The less sensitive to this disturbance is considered as the optimal identified value. The corresponding special virtual field is called hereafter *optimized* special virtual field.

4. Numerical simulations

4.1. Principle

The objective here is to investigate the capabilities of the VFM in terms of accuracy and stability. The input data are strain components on the top surface of bent plates. Such data are directly related to the curvatures within the framework of the theory of thin plates (Lekhnitskii, 1968). They can be obtained in practice with a suitable optical device, either directly or by differentiation of measured slopes (Surrel et al., 1999) but this point is not discussed here to focus only on the identification procedure. These data are therefore provided by a finite programme (ANSYS 6.0 package) and the goal is to retrieve the bending stiffness components input in the FE programme. The tested plate is a 0.1 m × 0.1 m square subjected to some local forces (see Fig. 2). The mesh has $50\times 50 = 2500$ square elements. F_1 causes bending of the plate along direction 1 between supports P_1 and P_2. F_2 causes bending of the plate along direction 2 between supports P_2 and P_3. A twist of the plate is finally caused by F_3.

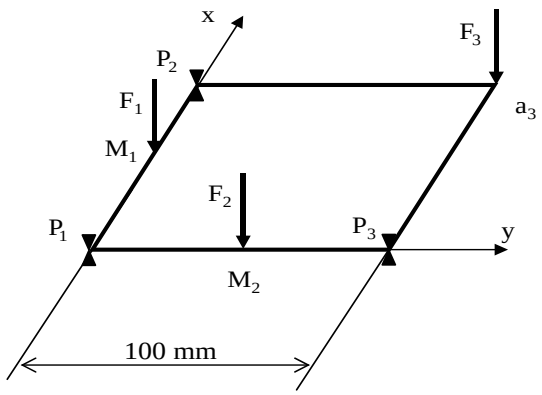

Fig. 2. Square plate under bending.

Table 2
Bending stiffnesses of different anisotropic plates

Plate #	Material	Stacking sequence	D_{xx} (N m)	D_{yy} (N m)	D_{xy} (N m)	D_{ss} (N m)	D_{xs} (N m)	D_{ys} (N m)
1	A	$[0_4]_s$	3.410	0.852	0.256	0.333	0	0
2	B	$[0_4]_s$	10.909	0.839	0.251	0.417	0	0
3	B	$[30_4]_s$	6.592	1.558	2.042	2.208	3.217	1.115
4	B	$[0 \pm 30\ 90]_s$	9.000	1.292	0.983	1.150	1.308	0.464
5	A	$[0 \pm 30\ 90]_s$	2.925	0.967	0.440	0.517	0.332	0.118

Consequently, the six bending stiffness components are expected to influence the actual deflection/slope/curvature fields. They are therefore identifiable. In practice, $F = F_1 = F_2 = F_3 = 10$ N.

Since the plate is simply supported at three points P_1, P_2 and P_3, $n_s = 3$ conditions must be written to obtain an admissible virtual field

$$\widehat{w}^*(x_{P_1}, y_{P_1}) = \widehat{w}^*(x_{P_2}, y_{P_2}) = \widehat{w}^*(x_{P_3}, y_{P_3}) = 0 \tag{18}$$

Concerning the numerical procedure, the first step is to fix a value for m and n which are the maximum degree of the monomials in Eq. (10). $m = 3$ and $n = 3$ are chosen here. In this case, $n_{\text{unk}} = 16$ A_{ij}'s must be determined to define the special virtual deflection field whereas $6 + n_s = 6 + 3 = 9$ equations are available. This result illustrates the fact that an infinity of solutions will be found a priori.

$$\frac{16!}{9!(16-9)!} = \frac{16!}{9!7!} = 11440$$

different square matrices can be extracted from the rectangular matrix **E** in Eq. (16). The procedure used in Grédiac et al. (2002a) and recalled in Section 3.4 is used to determine the A_{ij}'s. Since the side of the plate is 100 mm long, $a = b = 100$ mm in Eq. (10).

Several plates listed in Table 2 are tested. They exhibit various types of anisotropy. Material A is a glass/epoxy ($E_x = 40$ GPa, $E_y = 10$ GPa, $\nu_{xy} = 0.3$, $G_{xy} = 4$ GPa), material B is a carbon/epoxy ($E_x = 130$ GPa,

Table 3
Identified bending stiffnesses, plate 1

	D_{xx} (N m)	D_{yy} (N m)	D_{xy} (N m)	D_{ss} (N m)	D_{xs} (N m)	D_{ys} (N m)
Reference	3.410	0.852	0.256	0.333	0	0
Without noise	3.412	0.850	0.256	0.334	6.3×10^{-5}	-1.9×10^{-4}
	0.06%	*−0.23%*	*0%*	*0.3%*	–	–
$p = 1\%$	3.485	0.854	0.253	0.334	0.001	0.002
	−1.91%	*0.23%*	*−1.17%*	*0.30%*	–	–
$p = 5\%$	4.532	0.467	0.175	0.354	−0.016	0.002
	32.90%	*−45.19%*	*−31.64%*	*6.31%*	–	–
$q = 5\%$, average	3.430	0.840	0.267	0.333	4.4×10^{-4}	1.7×10^{-4}
	0.59%	*−1.41%*	*4.30%*	*0%*	–	–
$q = 5\%$, coef. of variation (%)	5.19	7.08	17.70	0.263	–	–

Table 4
Identified bending stiffnesses, plate 2

	D_{xx} (N m)	D_{yy} (N m)	D_{xy} (N m)	D_{ss} (N m)	D_{xs} (N m)	D_{ys} (N m)
Reference	10.909	0.839	0.251	0.417	0	0
Without noise	10.899	0.848	0.251	0.417	8.7×10^{-5}	0.01
	−0.09%	*1.07%*	*0%*	*0%*	–	–
$p = 1\%$	11.132	0.857	0.246	0.418	6.9×10^{-4}	−0.002
	2.04%	*2.15%*	*−1.99%*	*0.24%*	–	–
$p = 5\%$	12.616	1.281	0.100	0.432	−0.006	0.028
	15.65%	*52.68%*	*−60.16%*	*3.60%*	–	–
$q = 5\%$, average	11.031	8.347	0.234	4.189	15×10^{-4}	3.7×10^{-4}
	1.12%	*−0.47%*	*−6.77%*	*0.47%*	–	–
$q = 5\%$, coef. of variation (%)	8.23	12.79	76.66	0.986	–	–

$E_y = 10$ GPa, $v_{xy} = 0.3$, $G_{xy} = 5$ GPa). All plates are 1 mm thickness. Their bending stiffnesses in Table 2 are considered as reference values for the following numerical simulations.

4.2. Results

The results obtained for plates 1–5 are reported in Tables 3–7. In each case, several calculations have been performed.

- First, the three curvatures at the center of the elements obtained from the FE model are considered as input data. The values identified with such data are reported in row 2 of each Table (“without noise”). Note the deflections or the slopes could also be considered as input data but a numerical differentiation should be added. These cases are therefore not presently considered to focus only on the identification procedure.

Table 5
Identified bending stiffnesses, plate 3

	D_{xx} (N m)	D_{yy} (N m)	D_{xy} (N m)	D_{ss} (N m)	D_{xs} (N m)	D_{ys} (N m)
Reference	6.592	1.558	2.042	2.208	3.217	1.115
Without noise	6.614	1.564	2.051	2.222	3.234	1.143
	0.33%	*0.39%*	*0.44%*	*0.63%*	*0.53%*	*2.51%*
$p = 1\%$	6.397	1.589	2.015	2.193	3.268	1.159
	−2.96%	*1.99%*	*−1.32%*	*−0.68%*	*1.59%*	*3.95%*
$p = 5\%$	4.874	2.244	1.421	2.743	3.813	1.349
	−26.06%	*42.75%*	*−30.41%*	*24.23%*	*18.53%*	*20.99%*
$q = 5\%$, average	6.656	1.590	2.135	2.219	3.214	1.159
	0.97%	*2.05%*	*4.55%*	*0.50%*	*−0.09%*	*3.95%*
$q = 5\%$, coef. of variation (%)	10.1	29.0	23.0	11.1	9.1	37.7

Table 6
Identified bending stiffnesses, plate 4

	D_{xx} (N m)	D_{yy} (N m)	D_{xy} (N m)	D_{ss} (N m)	D_{xs} (N m)	D_{ys} (N m)
Reference	9.000	1.292	0.983	1.150	1.308	0.464
Without noise	9.006	1.295	0.982	1.146	1.308	0.464
	0.07%	*0.23%*	*−0.10%*	*−0.35%*	*0%*	*0%*
$p = 1\%$	8.954	1.314	0.969	1.143	1.296	0.484
	−0.51%	*1.70%*	*−1.42%*	*−0.61%*	*−0.92%*	*4.31%*
$p = 5\%$	10.289	1.765	0.204	1.052	1.208	0.622
	14.32%	*36.61%*	*−79.25%*	*−8.52%*	*−7.65%*	*34.05%*
$q = 5\%$, average	8.964	1.309	0.986	1.166	1.296	0.475
	−0.40%	*1.32%*	*0.31%*	*1.39%*	*−0.92%*	*2.37%*
$q = 5\%$, coef. of variation (%)	4.47	10.80	18.42	3.50	7.29	9.66

Table 7
Identified bending stiffnesses, plate 5

	D_{xx} (N m)	D_{yy} (N m)	D_{xy} (N m)	D_{ss} (N m)	D_{xs} (N m)	D_{ys} (N m)
Reference	2.925	0.967	0.440	0.517	0.332	0.118
Without noise	2.933	0.972	0.439	0.517	0.331	0.120
	0.27%	*0.52%*	*−0.23%*	*0%*	*−0.30%*	*1.69%*
$p = 1\%$	2.981	1.001	0.430	0.504	0.340	0.130
	1.91%	*3.52%*	*−2.27%*	*−2.51%*	*2.41%*	*10.17%*
$p = 5\%$	3.986	1.717	0.394	0.452	0.326	0.271
	36.27%	*77.56%*	*−10.45%*	*−12.57%*	*−1.81%*	*129.66%*
$q = 5\%$, average	2.899	0.959	0.336	0.516	0.436	0.120
	−0.89%	*−0.83%*	*−23.64%*	*−0.19%*	*31.33%*	*1.69%*
$q = 5\%$, coef. of variation (%)	6.25	10.15	6.81	0.82	6.61	5.66

- Two types of noise are then added to these input data to observe the sensitivity of the procedure to a noise. The first one is a shift of the coordinates of a magnitude of $p\%$ of the side of the square plate. In practice, such bias could be due to a displacement of the camera which captures the data onto the surface of the plate. In this case, a constant value of $p \times a$ is added to the coordinates of the points where the data are known (the center of the elements of the FE model): $x \to x + p \times a$, $y \to y + p \times a$. Results obtained with $p = 1\%$ and $p = 5\%$ are reported in rows 3 and 4 of each table. The second type of noise is a uniform random noise added to the curvatures. The magnitude is a percentage $q\%$ of the maximum value of the absolute value of the three curvatures. Results obtained with $q = 5\%$ are reported in rows 5 and 6 of each table. Thirty different calculations have been performed, each of them with a new set of randomly generated noisy curvatures. The average of each stiffness is reported in row 5. The coefficient of variation (defined by the ratio between the standard deviation of the distribution and the average) is reported in row 6.

When looking at the results obtained from "exact" data, the identified stiffnesses are all within less than 1% of the reference ones, validating the numerical identification routine. To evaluate the impact of simulated measurement noise, one has to look at the results in a comparative manner. Comparing the results obtained for plate 1 (glass/epoxy unidirectional) and plate 2 (carbon/epoxy unidirectional), it appears quite clearly that the second is more sensitive to noise than the first. This is consistent with results obtained on in-plane configurations (Pierron and Grédiac, 2000) where a stronger anisotropy leads to more difficult identification. Nevertheless, the results are good in general, apart from the D_{xy} term which is very sensitive to noise. Again, this is consistent with previous results obtained by the authors or others teams. The reason is that this stiffness component does not influence the strain and stress fields very much, leading to a certain instability. A possible way out of this is to identify invariant parameters, as proposed in Grédiac (1996a). Another surprising feature is the sensitivity of the identified stiffness components in this case to a severe shift in coordinates ($p = 5\%$), except D_{ss}. This had not been seen on previous in-plane configurations (Pierron and Grédiac, 2000). The reason is certainly the fact that the shear strain is presently predominant in the actual strain field because of the loading conditions, as illustrated below. Finally, it can be seen that the coupling terms D_{xs} and D_{ys} are always at least an order of magnitude below the other terms, indicating that these terms are zero. Considering now the carbon/epoxy unidirectional plate at 30° it can be seen that although both terms are identified within reasonable bounds, the D_{ys} component is more sensitive to noise. The reason is certainly the same as that given above for the D_{xy} component. Nevertheless, the present procedure enables the extraction of the six stiffness components of an anisotropic plate with just one test. Moving now to more elaborate stacking sequences (Tables 6 and 7), the same remarks as above apply.

4.3. Examples of special virtual fields

The special virtual fields obtained for plate 1 are plotted in Fig. 3 along with the actual deflection field. The special virtual fields are multiplied by a constant K to obtain comparable orders of magnitudes between actual and virtual fields. K is reported in the caption of the figures. It can be observed that both the actual and the virtual deflections are zero at the three supports. The virtual deflections are zero at these points because they are kinematically admissible. It also clearly appears that the actual deflection field is much smoother than the special virtual fields. This is due to the fact that the virtual fields filter the actual curvatures to extract the unknown parameters. Consequently, the measured data at some parts of the plate contribute more than others. As a general remark, it is clear that such fields could not have been guessed. Their expressions are given below.

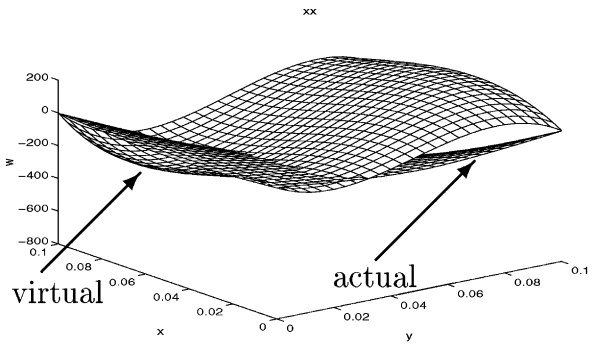

(a) Actual and special virtual field for D_{xx} : $\widehat{w}^{*(1)}$
$K = 3 \times 10^3$

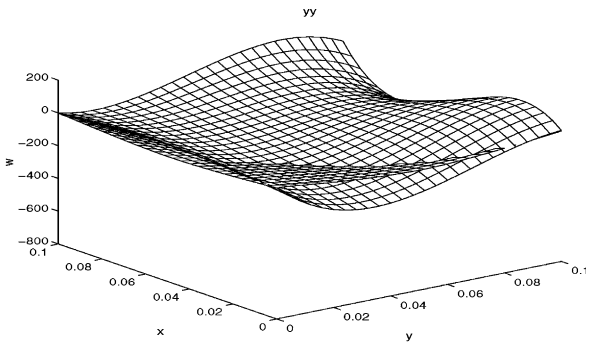

(b) Actual and special virtual field for D_{yy} : $\widehat{w}^{*(2)}$
$K = 10 \times 10^3$

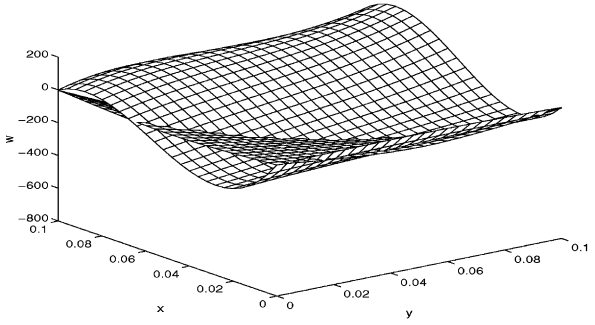

(c) Actual and special virtual field for D_{xy} : $\widehat{w}^{*(3)}$
$K = 50 \times 10^3$

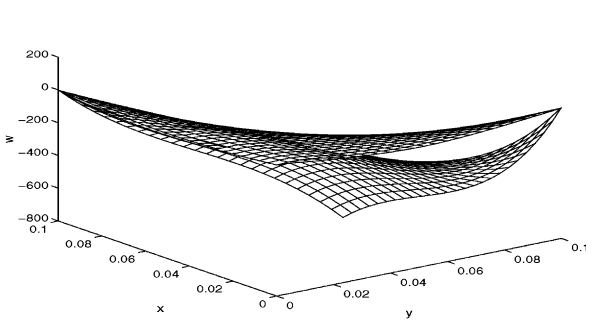

(d) Actual and special virtual field for D_{ss} : $\widehat{w}^{*(4)}$
$K = 400 \times 10^3$

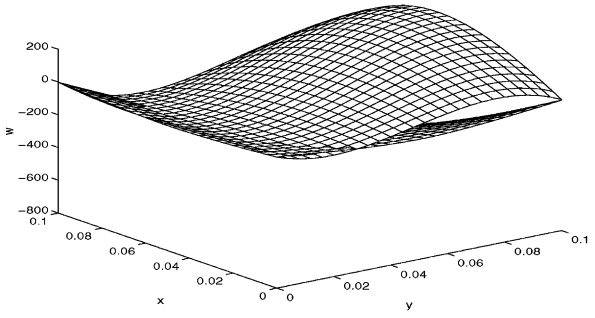

(e) Actual and special virtual field for D_{xs} : $\widehat{w}^{*(5)}$
$K = 150 \times 10^3$

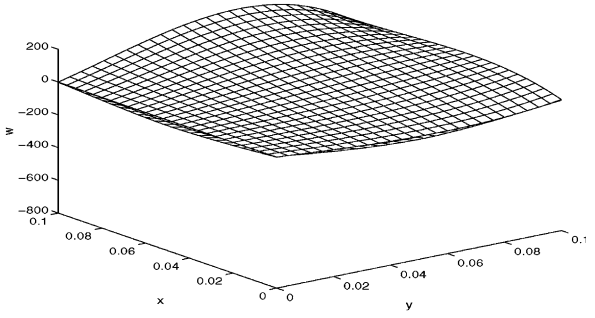

(f) Actual and special virtual fields for $D_{ys}^{(3)}$: $\widehat{w}^{*(6)}$
$K = 50 \times 10^3$

Fig. 3. Actual deflection field (same in each figure) and optimized special virtual deflection fields, plate 1.

$$
\begin{cases}
\widehat{w}^{*(1)}(x,y) = -0.2933\dfrac{y}{a} + 0.9345\dfrac{y^2}{a^2} - 0.6412\dfrac{y^3}{a^3} + 0.0512\dfrac{x}{a} + 0.2274\dfrac{xy^2}{a^3} \\
\qquad -0.4594\dfrac{x^2}{a^2} + 0.4082\dfrac{x^3}{a^3} - 0.2301\dfrac{x^3y}{a^4} \\
\widehat{w}^{*(2)}(x,y) = -0.1554\dfrac{y}{a} + 0.3005\dfrac{y^2}{a^2} - 0.1451\dfrac{y^3}{a^3} + 0.0093\dfrac{x}{a} + 0.1110\dfrac{xy}{a^2} \\
\qquad -0.4175\dfrac{x^2y^2}{a^4} - 0.0093\dfrac{x^3}{a^3} + 0.3153\dfrac{x^3y^2}{a^5} \\
\widehat{w}^{*(3)}(x,y) = 0.0011\left(\dfrac{y}{a} - \dfrac{y^2}{a^2}\right) - 0.0406\dfrac{x}{a} + 0.0091\dfrac{xy}{a^2} + 0.0965\dfrac{x^2}{a^2} + 0.0143\dfrac{x^2y^3}{a^5} \\
\qquad -0.0559\dfrac{x^3}{a^3} - 0.0231\dfrac{x^3y^2}{a^5} \\
\widehat{w}^{*(4)}(x,y) = 0.0004\dfrac{y}{a} - 0.0042\dfrac{y^2}{a^2} + 0.0038\dfrac{y^3}{a^3} - 0.0003\dfrac{x}{a} - 0.0063\dfrac{xy^3}{a^4} \\
\qquad +0.0077\dfrac{x^2y^2}{a^4} + 0.0003\dfrac{x^3}{a^3} - 0.0043\dfrac{x^3y}{a^4} \\
\widehat{w}^{*(5)}(x,y) = -0.0045\dfrac{y}{a} + 0.0145\dfrac{y^2}{a^2} - 0.0100\dfrac{y^3}{a^3} + 0.0013\dfrac{xy}{a^2} + 0.0039\dfrac{xy^2}{a^3} \\
\qquad -0.0015\dfrac{x^2}{a^2} + 0.0015\dfrac{x^3}{a^3} - 0.0052\dfrac{x^3y}{a^4} \\
\widehat{w}^{*(6)}(x,y) = 0.0026\left(\dfrac{y^3}{a^3} - \dfrac{y}{a}\right) + 0.0001\left(\dfrac{x^3}{a^3} - \dfrac{x}{a}\right) + 0.0092\dfrac{xy}{a^2} + 0.0020\dfrac{x^2y}{a^3} \\
\qquad -0.0169\dfrac{x^2y^3}{a^5} + 0.0068\dfrac{x^3y^2}{a^5}
\end{cases}
\tag{19}
$$

It can be observed that the monomials in the expansion of the special virtual fields are different from one case to another even though y/a and x^3/a^3 are used in the six cases.

Actual and virtual curvatures k_x and $\widehat{k}_x^{*(1)}$ are plotted in Fig. 4a and b respectively, their product $k_x \times \widehat{k}_x^{*(1)}$ in Fig. 4c. Two cases are considered: without noise added to the curvatures (left-hand side column) and with noise added to the curvatures (right-hand side column). The second case is in fact the result obtained with the first of the 30 calculations performed when noisy curvatures are processed (see Section 4.2 above). The magnitude of the noise is here $q = 5\%$ of the maximum value of the absolute value of the three curvatures. In the present case, the maximum value of the absolute value of the third curvature k_s is about 30 times greater than the maximum value of the absolute value of the first curvature k_x. This is due to the fact that $F = F_1 = F_2 = F_3$ in Fig. 2, leading therefore to a predominant twist. This is the reason why the error on k_x is very crude, as can be seen in Fig. 4a.

The virtual curvature $\widehat{k}_x^{*(1)}$ is rather simple. This result is consistent with the above expression of the special virtual deflection field: only $1/a^2$, x/a^3 and xy/a^4 are used to expand the virtual strain $\widehat{k}_x^{*(1)}$ in the case "without noise". It must be pointed out that the virtual curvature fields are similar in both cases.

In both cases too, it can be checked that

$$\int_S k_x \widehat{k}_x^{*(1)} \mathrm{d}S = 1 \tag{20}$$

since $\widehat{k}_x^{*(1)}$ is a *special* virtual field.

The identified rigidities are directly proportional to the virtual deflection at M_1, M_2 and M_3. It can be checked in Fig. 5 that the virtual deflection is about the same in both cases (actual curvatures "without

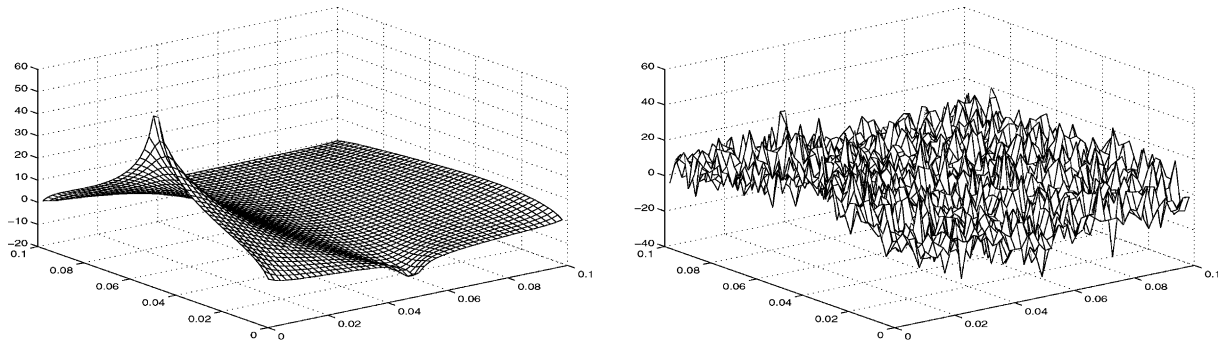

(a) Actual curvature field k_x

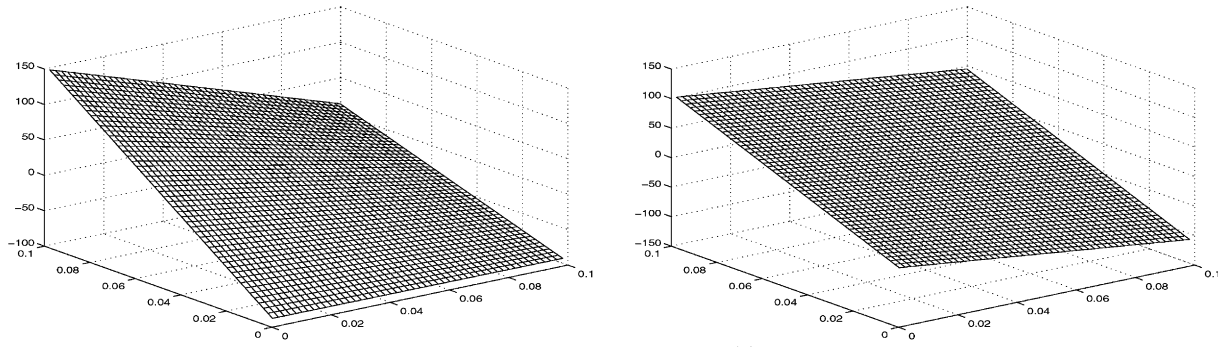

(b) Virtual curvature field $\widehat{k}_x^{*(1)}$

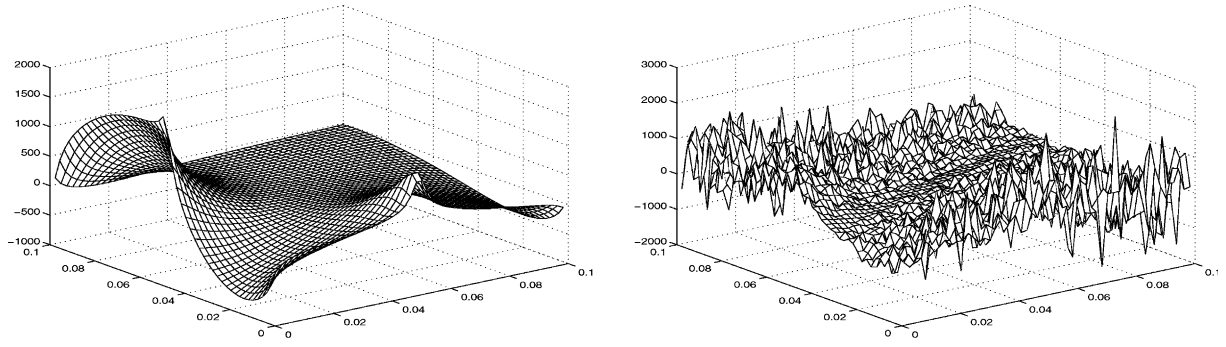

(c) Product actual $\times$ virtual field $k_x \times \widehat{k}$

Fig. 4. Actual and optimized special virtual curvature fields without (left-hand side column) and with (right-hand side column) noise, $q = 5\%$, plate 1.

noise'' and ''with noise''). The identified value of D_{xx} is therefore close from one case to another. Indeed, the identified value for D_{xx} is 3.152 N m in the case ''with noise'' and 3.412 N m in the case ''without noise'' (the reference value is 3.410 N m). This clearly illustrate the stability of the procedure. In fact, the local values of the curvature exhibit an important random error at each point, but the integration average out these local discrepancies between actual and noisy data.

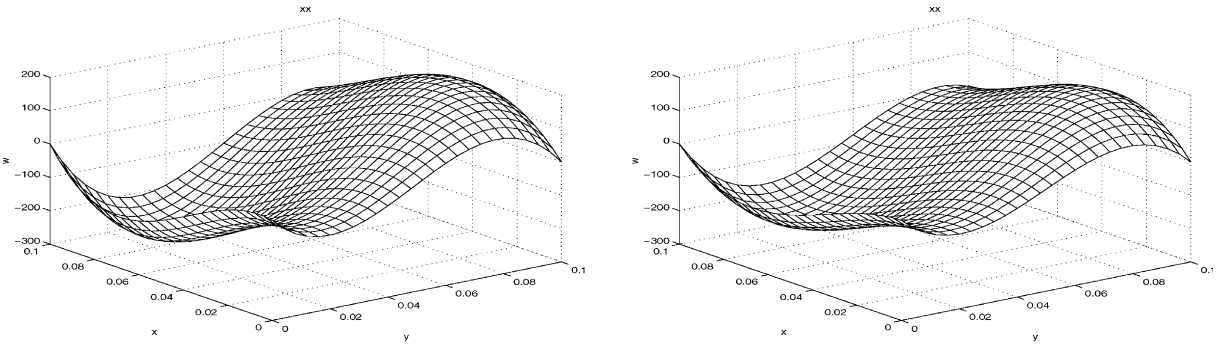

(a) without noise (b) with noise, $q = 5\%$

Fig. 5. Optimized special virtual deflection field $\widehat{w}^{*(1)}$, actual curvature without and with noise, $q = 5\%$, plate 1.

4.4. Open hole plate

An important feature of the method is that it can be adapted to a plate regardless of its geometry. As an example, an open hole plate has been simulated (see Fig. 6). The plate has the same dimensions as the previous ones, but has a 20×20 mm^2 square open hole in its center. The material used here is the glass/epoxy unidirectional composite. The results of the identification are reported in Table 8. Comparing to the results concerning the same material and the normal square plate (Table 3), it can be seen that both D_{yy} and D_{ss} are now much more sensitive to simulated noise. This indicates that now, the mechanical test used is not so well suited to extract all the stiffness components. One way to approach this issue is proposed by Le-Magorou et al. (2002) and Arafeh et al. (1995) where the test configuration is optimized using sensitivity coefficients obtained by a finite element model. Since these authors use finite element model updating, it is natural for them to extract sensitivity factors from these models. Nevertheless, the VFM should be able to provide information on the "identifiability" of the different coefficients directly from the curvature maps.

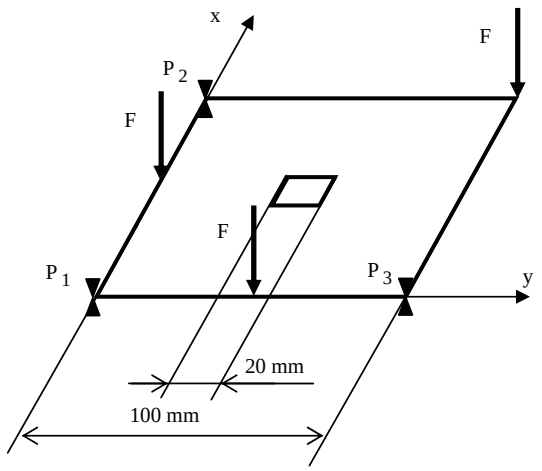

Fig. 6. Open hole plate.

Table 8
Identified bending stiffnesses, open hole plate

	D_{xx} (N m)	D_{yy} (N m)	D_{xy} (N m)	D_{ss} (N m)	D_{xs} (N m)	D_{ys} (N m)
Reference	3.410	0.852	0.256	0.333	0	0
Without noise	3.412	0.854	0.255	0.333	4.8×10^{-4}	8.7×10^{-5}
	0.06%	*0.23%*	*−0.39%*	*0%*	–	–
$p = 1\%$	3.380	1.104	0.245	0.333	-3.3×10^{-4}	0.026
	−0.88%	*29.58%*	*−4.29%*	*0%*	–	–
$p = 5\%$	3.239	2.057	0.140	0.340	−0.086	0.125
	−5.01%	*141.43%*	*2.10%*	*−45.31%*	–	–
$q = 5\%$, average	3.342	0.847	0.270	0.334	-8.2×10^{-4}	0.002
	−0.02%	*−0.59%*	*0.30%*	*5.47%*	–	–
$q = 5\%$, coef. of variation (%)	7.18	27.08	0.15	22.44	–	–

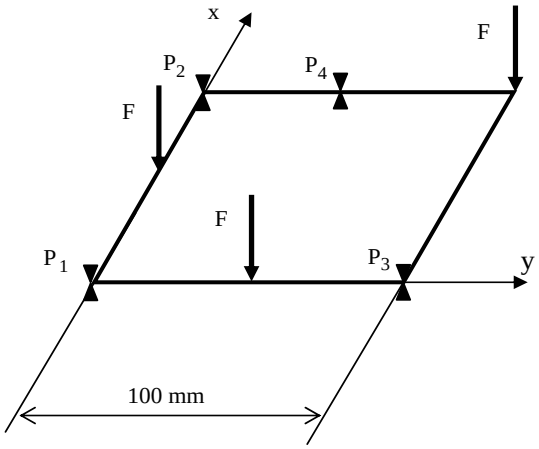

Fig. 7. Hyperstatic plate.

Table 9
Identified bending stiffnesses, hyperstatic plate

	D_{xx} (N m)	D_{yy} (N m)	D_{xy} (N m)	D_{ss} (N m)	D_{xs} (N m)	D_{ys} (N m)
Reference	3.410	0.852	0.256	0.333	0	0
Without noise	3.411	0.853	0.256	0.334	2.4×10^{-5}	2.3×10^{-4}
	0.03%	*0.12%*	*0%*	*0.30%*	–	–
$p = 1\%$	3.393	0.848	0.254	0.336	−0.001	7.2×10^{-4}
	−0.50%	*−0.47%*	*−0.78%*	*0.90%*	–	–
$p = 5\%$	3.337	0.839	0.257	0.359	−0.019	0.003
	−2.14%	*−1.53%*	*0.39%*	*7.81%*	–	–
$q = 5\%$, average	3.413	0.852	0.256	0.334	5.6×10^{-5}	1.6×10^{-4}
	0.09%	*0%*	*0%*	*0.30%*	–	–
$q = 5\%$, coef. of variation (%)	1.94	1.48	5.48	0.54	–	–

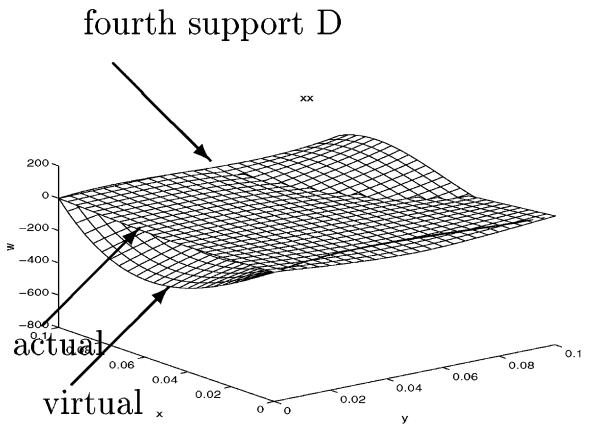

(a) Actual and special virtual field for D_{xx} : $\widehat{w}^{*(1)}$
$K = 7 \times 10^3$

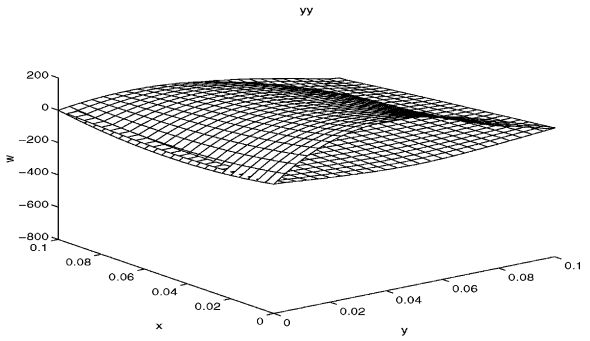

(b) Actual and special virtual field for D_{yy} : $\widehat{w}^{*(2)}$
$K = 13 \times 10^3$

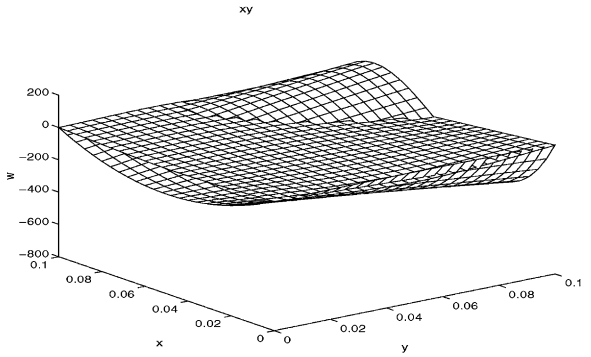

(c) Actual and special virtual field for D_{xy} : $\widehat{w}^{*(3)}$
$K = 70 \times 10^3$

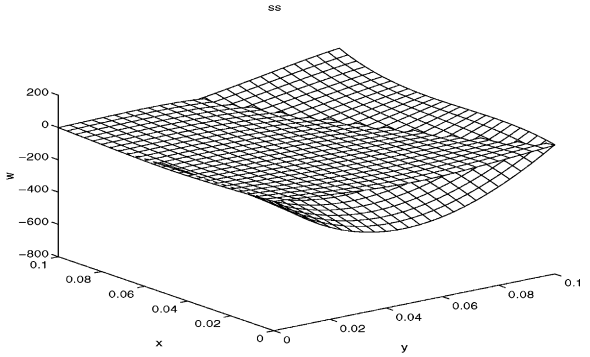

(d) Actual and special virtual field for D_{ss} : $\widehat{w}^{*(4)}$
$K = 60 \times 10^3$

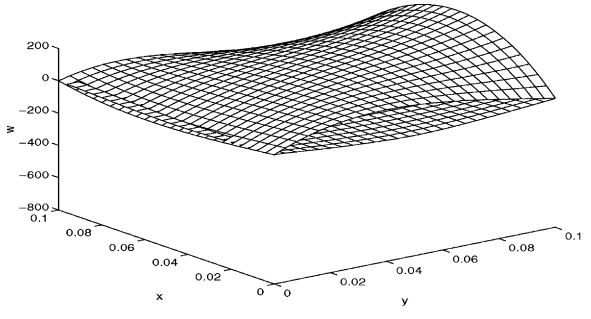

(e) Actual and special virtual field for D_{xs} : $\widehat{w}^{*(5)}$
$K = 80 \times 10^3$

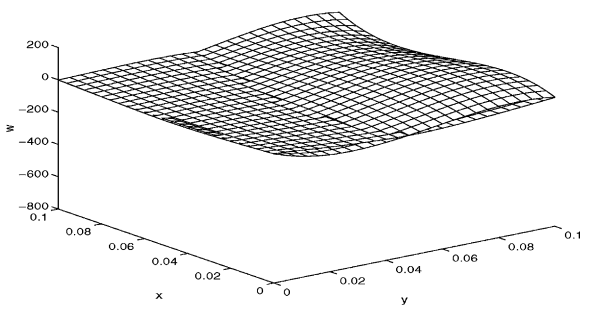

(f) Actual and special virtual fields for $D_{ys}^{(3)}$: $\widehat{w}^{*(6)}$
$K = 100 \times 10^3$

Fig. 8. Actual deflection field (same in each figure) and optimized special virtual deflection fields, hyperstatic plate.

More work is needed in this area to perform the simultaneous optimization of both actual and virtual fields. This is a key issue for the future of identification from whole-field measurements with his procedure.

4.5. Hyperstatic plate

A last example is shown to illustrate the capabilities of the method. A fourth support is added at point P_4, as shown in Fig. 7. If this test is carried out in practice, it will be impossible to know the actual imposed displacement at this fourth support. For the numerical simulations, an imposed value of 0.5 mm is prescribed at this fourth support to model a small defect of the testing device. It should be underlined that if a finite element model updating technique was used, the value of this imposed displacement would be required as input data. With the VFM, only a fourth condition must be added to the three listed in Eq. (18) to obtain admissible deflection fields

$$\widehat{w}^*(x_{P_4}, y_{P_4}) = 0 \tag{21}$$

In this case, the contribution to the virtual work of the force at this point is zeroed by the virtual deflection. The material use here is the glass/epoxy unidirectional. The results are reported in Table 9. When comparing to Table 3 (same material), it is clear that the results are indeed much better with the fourth support. This indicates with no error that this last test is better in terms of sensitivity. It shows that the VFM could be used to extract sensitivity factors based on simulated noise. Again, this point should be investigated more closely in future work.

Finally, Fig. 8 shows both actual and virtual fields. It can be checked that the virtual fields have all zero deflection at point P_4 since it is admissible.

5. Conclusion

Applying the VFM with special virtual fields leads to the direct determination of the bending rigidities of thin anisotropic plates from heterogeneous strain fields. A procedure for determining the special virtual fields has been presented in the particular case of the bending of plates. Numerical simulations have shown that the procedure is accurate. The sensitivity of the identified parameters to noisy data has been investigated. It has been shown that it is compatible with a practical implementation of the procedure since the noise is unavoidable in this case. Finally, the VFM has been tested in the case of an hyperstatic plate for which the displacements prescribed by the supports remain generally unknown. The results found in this case are much less sensitive to noise than in the other cases. This feature clearly shows that the actual strain field (and not only the virtual one) directly influences the accuracy and the sensitivity of the procedure. More work is therefore needed to define some parameters to evaluate the sensitivity of each stiffness component to the identification procedure. This could lead in the future to the definition of a confidence index for each value identified and to the definition of mechanical configurations which would be optimized with respect to this index.

References

Arafeh, M.H., Knopf-Lenoir, C., Rouger, F., 1995. Conception optimale d'essais de flexion de plaques orthotropes et identification. Comptes Rendus de l'Académie des Sciences II/321, 351–354.

Araujo, A.L., Soares, C.M.M., Freitas, M.J.M., 1996. Characterization of material parameters of composite specimens using optimization and experimental data. Composites Part B 27 (2), 185–191.

Ayorinde, E., Gibson, R., 1993. Elastic constants of orthotropic composite materials using plate resonance frequencies, classical lamination theory and an optimized three-mode Rayleigh formulation. Composites Engineering 3 (5), 395–407.

Deobald, L., Gibson, R., 1988. Determination of elastic constants of orthotropic plates by a modal analysis/Rayleigh–Ritz technique. Journal of Sound and Vibration 124 (2), 269–283.

DeWilde, W.P., 1990. Identification of the rigidities of composite systems by mixed numerical/experimental techniques. In: Mechanical Identification of Composites. Elsevier, pp. 1–15.

Frederiksen, P.S., 1997. Numerical studies for identification of orthotropic elastic constants of thick plates. European Journal of Mechanics A/Solids 16, 117–140.

Golub, G.H., Loan, C.F.V., 1993. Matrix Computations, third ed. The Johns Hopkins University Press.

Grédiac, M., 1989. Principe des travaux virtuels et identification/principle of virtual work and identification. Comptes Rendus de l'Académie des Sciences II/309, 1–5, Gauthier-Villars, in French with Abridged English Version.

Grédiac, M., 1996a. On the direct determination of invariant parameters governing the bending of anisotropic plates. International Journal of Solids and Structures 33 (27), 3969–3982.

Grédiac, M., 1996b. The use of heterogeneous strain fields for the characterization of composite materials. Composite Science and Technology 56, 841–846.

Grédiac, M., Pierron, F., 1998. A T-shaped specimen for the direct characterization of orthotropic materials. International Journal for Numerical Methods in Engineering 41, 293–309.

Grédiac, M., Pierron, F., 2001. Numerical issues in the virtual fields method. International Journal for Numerical Methods in Engineering, submitted for publication.

Grédiac, M., Vautrin, A., 1990. A new method for determination of bending rigidities of thin anisotropic plates. Journal of Applied Mechanics 57, 964–968.

Grédiac, M., Pierron, F., Surrel, Y., 1999. Novel procedure for complete in-plane composite characterization using a T-shaped specimen. Experimental Mechanics 39 (2), 142–149.

Grédiac, M., Auslender, F., Pierron, F., 2001. Applying the virtual fields method to determine the through-thickness moduli of thick composites with a nonlinear shear response. Composites/PartA 32 (12), 1713–1725.

Grédiac, M., Toussaint, E., Pierron, F., 2002a. Special virtual fields for the direct determination of material parameters with the virtual fields method. 1—principle and definition. International Journal of Solids and Structures 39, 2691–2705.

Grédiac, M., Toussaint, E., Pierron, F., 2002b. Special virtual fields for the direct determination of material parameters with the virtual fields method. 2—application to in-plane properties. International Journal of Solids and Structures 39, 2707–2730.

Hendricks, M.A.N., 1991. Identification of the mechanical properties of solid materials. Doctoral dissertation, Eindhoven University of Technology.

Lekhnitskii, S.G., 1968. Anisotropic Plates. Gordon and Breach.

LeMagorou, L., Bos, F., Rouger, F., 2002. Identification of constitutive laws for wood-based panels by means of an inverse method. Composite Science and Technology 62 (4), 591–596.

Meuwissen, M.H.H., Oomens, C.W.J., Baaijens, F.P.T., Petterson, R., Janssen, J.D., 1998. Determination of the elasto-plastic properties of aluminium using a mixed numerical-experimental method. Journal of Materials Processing Technology 75, 204–211.

Mota Soares, C., Moreira de Freitas, M., Araújo, A.L., Pedersen, P., 1993. Identification of material properties of composite plate specimens. Composite Structures 25, 277–285.

Okada, H., Fukui, Y., Kumazawa, N., 1999. An inverse analysis determining the elastic-plastic stress–strain relationship using nonlinear sensitivities. Computer Modeling and Simulation in Engineering 4 (3), 176–185.

Pierron, F., Grédiac, M., 2000. Identification of the through-thickness moduli of thick composites from whole-field measurements using the Iosipescu fixture: theory and simulations. Composites: Part A 31 (4), 309–318.

Pierron, F., Zhavaronok, S., Grédiac, M., 2000. Identification of the through-thickness properties of thick laminates using the virtual fields method. International Journal of Solids and Structures 37 (32), 4437–4453.

Sol, H., 1986. Identification of anisotropic plate rigidities using free vibration data. Doctoral dissertation, University of Brussels.

Surrel, Y., Fournier, N., Grédiac, M., Paris, P.A., 1999. Phase-stepped deflectometry applied to shape measurement of bent plates. Experimental Mechanics 39 (1), 66–70.

Wang, W.T., Kam, T.Y., 2001. Elastic constants identification of shear deformable laminated composite plates. Journal of Engineering Mechanics 127 (11), 1117–1123.